THE JOURNAL OF BIOLOGICAL CHEMISTRY VOL. 287, NO. 51, pp. 42984–42994, December 14, 2012

Motor Neuron-specific Disruption of Proteasomes, but Not Autophagy, Replicates Amyotrophic Lateral Sclerosis*[S]

Received for publication, September 8, 2012, and in revised form, October 18, 2012 Published, JBC Papers in Press, October 24, 2012, DOI 10.1074/jbc.M112.417600

Yoshitaka Tashiro,[1,a] Makoto Urushitani,[1,b] Haruhisa Inoue,[c] Masato Koike,[d] Yasuo Uchiyama,[d] Masaaki Komatsu,[e] Keiji Tanaka,[f] Maya Yamazaki,[g] Manabu Abe,[g] Hidemi Misawa,[h] Kenji Sakimura,[g] Hidefumi Ito,[2,i] and Ryosuke Takahashi[aj,3]

From the [a]Department of Neurology, Kyoto University Graduate School of Medicine, Kyoto 6068507, Japan, the [b]Unit for Neurobiology and Therapeutics, Molecular Neuroscience Research Center, Shiga University of Medical Science, Shiga 5202192, Japan, the [c]Center for iPS Cell Research and Application, Institute for Integrated Cell-Material Sciences, Kyoto University, Kyoto 6068507, Japan, the [d]Department of Cell Biology and Neuroscience, Juntendo University Graduate School of Medicine, Tokyo 1138421, Japan, the [e]Protein Metabolism Project, Tokyo Metropolitan Institute of Medical Science, Tokyo 1568506, Japan, the [f]Tokyo Metropolitan Institute of Medical Science, 1-6, Tokyo 1568506, Japan, the [g]Department of Cellular Neurobiology, Brain Research Institute, Niigata University, Niigata 9518585, Japan, the [h]Department of Pharmacology, Faculty of Pharmacy, Keio University, Tokyo 1058512, Japan, the [i]Department of Neurology, Wakayama Medical University Graduate School of Medicine, Wakayama 6418510, Japan, and the [j]Core Research for Evolutional Science and Technology (CREST), Japan Science, and Technology Agency, Saitama 3320012, Japan

Background: It is not clear how protein degradation systems are involved in ALS pathogenesis.
Results: Transgenic mice with motor neuron-specific knock-out of proteasomes, but not of autophagy showed ALS phonotypes.
Conclusion: Dysfunction of proteasome may primarily contribute to the pathogenesis of ALS than that of autophagy.
Significance: Modulation of proteasome function is a promising approach toward treatment of ALS.

Evidence suggests that protein misfolding is crucially involved in the pathogenesis of amyotrophic lateral sclerosis (ALS). However, controversy still exists regarding the involvement of proteasomes or autophagy in ALS due to previous conflicting results. Here, we show that impairment of the ubiquitin-proteasome system, but not the autophagy-lysosome system in motor neurons replicates ALS in mice. Conditional knock-out mice of the proteasome subunit Rpt3 in a motor neuron-specific manner (Rpt3-CKO) showed locomotor dysfunction accompanied by progressive motor neuron loss and gliosis. Moreover, diverse ALS-linked proteins, including TAR DNA-binding protein 43 kDa (TDP-43), fused in sarcoma (FUS), ubiquilin 2, and optineurin were mislocalized or accumulated in motor neurons, together with other typical ALS hallmarks such as basophilic inclusion bodies. On the other hand, motor neuron-specific knock-out of Atg7, a crucial component for the induction of autophagy (Atg7-CKO), only resulted in cytosolic accumulation of ubiquitin and p62, and no TDP-43 or FUS pathologies or motor dysfunction was observed. These results strongly suggest that proteasomes, but not autophagy, fundamentally govern the development of ALS in which TDP-43 and FUS proteinopathy may play a crucial role. Enhancement of proteasome activity may be a promising strategy for the treatment of ALS.

Amyotrophic lateral sclerosis (ALS)[4] is a fatal neurodegenerative disorder characterized by progressive loss of upper and motor neurons. Although the exact pathogenesis of ALS remains elusive, prior studies of causal genes for familial ALS, including superoxide dismutase 1 (SOD1) (1), als2 (2), TAR DNA-binding protein 43 kDa (TDP-43) (3, 4), fused in sarcoma (FUS) (5, 6), and optineurin (7), have identified diverse pathogenic cascades and key molecules both *in vitro* and *in vivo* (8). In particular, accumulation of ubiquitinated inclusions containing these gene products is a common feature in most familial ALS models and is also a pathologic hallmark of sporadic ALS

* This work was supported by Grants-in-Aid for scientific research from the Japan Society for the Promotion of Science (21500336 and 24300132), Grants-in-Aid for scientific research on Innovative Areas Foundation of Synapse and Neurocircuit Pathology (22110007), Brain Environment (23111002), and Comprehensive Brain Science Network) from the Ministry of Education, Culture, Sports, Science and Technology of Japan, Funding Program for Next Generation World-Leading Researchers (L132), the Japan Science and Technology Agency (AS2211173G), the Research Committee of CNS Degenerative Diseases and Comprehensive Research on Disability Health and Welfare, the Ministry of Health, Labour and Welfare of Japan, Japan Science and Technology Agency, and Core Research for Evolutional Science and Technology.
[S] This article contains supplemental Table S1 and Fig. S1.
[1] Both authors contributed equally to this work.
[2] To whom correspondence may be addressed: Department of Neurology, Wakayama Medical University Graduate School of Medicine, 811-1, Kimiidera, Wakayama 6418510, Japan. Tel.: +81-73-441-0654; Fax: +81-73-447-9488; E-mail: ito@wakayama-med.ac.jp.
[3] To whom correspondence may be addressed: Dept. of Neurology, Kyoto University Graduate School of Medicine, 54 Shogoin-Kawaharacho, Sakyoku, Kyoto 6068507, Japan. Tel.: +81-75-751-4397; Fax: +81-75-761-9780; E-mail: ryosuket@kuhp.kyoto-u.ac.jp.

[4] The abbreviations used are: ALS, amyotrophic lateral sclerosis; 3-MA (3-methyladenine), Atg (autophagy-related protein), CAG (chicken β-actin promoter with cytomegalovirus enhancer), ChAT (choline acetyltransferase), CKO (conditional knockout), Cre (cyclization recombination enzyme), FRT (flippase recognition target), LC3-II (light chain 3-II), loxP (locus of crossing over P1), MAC-2 (macrophage antigen-2), Nbr1 (neighbor of BRCA1), Neo (neomycin resistance gene), Rpn (regulatory particle non-ATPase subunit), Rpt (regulatory particle triple-ATPase subunit), SOD1 (superoxide dismutase 1), SQSTM1 (sequestosome 1), UCH-L1 (ubiqitin carboxy-terminal hydrolase L1), UPS (ubiquitin-proteasome system), VAChT (vesicular acetylcholine transporter).

(9, 10), indicating that failure to eliminate detrimental proteins is linked to pathogenesis of both types of ALS.

Protein quality control is a vital system for regulating cellular homeostasis and is mediated by two major pathways: the ubiquitin-proteasome system (UPS) and the autophagy-lysosome system. The impairment of either is implicated in the neurodegeneration seen in ALS, Parkinson disease, Alzheimer disease, and polyglutamine disease (11, 12) by allowing toxic proteins to accumulate in neurons or glial cells (13, 14). For instance, genetic mutations in Parkin (the ubiquitin ligase) and UCH-L1 (the enzyme for de-ubiquitination) are reported to cause Parkinson disease (15–17). Moreover, ablation of the *Parkin* gene in transgenic mice expressing its substrate, the Pael receptor, results in progressive nigral degeneration, similar to Parkinson disease (18). Furthermore, dopaminergic neuron-specifc gene knock-out of Rpt2, a 26S proteasome subunit in mice, resulted in dopaminergic neurodegneratrion accompanied by Pale body-like inclusion composed of alpha-synuclein (19). A role for autophagy has also been shown in Parkinson disease, Alzheimer disease, and Huntington disease (20, 21). Indeed, suppression of autophagy in neuronal cells induces neurodegeneration with robust ubiquitinated inclusions (22, 23).

In ALS, the presence of ubiquitinated inclusions such as skein-like and round hyaline inclusions strongly suggests dysfunction of the UPS. Indeed, we have shown that continuous expression of mutant SOD1 results in decreased proteasome activity, and that primary cultured embryonic motor neurons are vulnerable to proteasome inhibition by lactacystin (24). On the contrary, other reports have documented that proteasome activity is unchanged (25) or increased (26, 27), and it has been reported that long-term pharmacological inhibition of proteasomes does not cause motor neuron death in a slice culture study (28). Besides proteasomes, autophagy is implicated in the pathogenesis of ALS as well. Mutant SOD1 and TDP-43 are reportedly degraded by the autophagy-lysosome system, as well as by the proteasome (29, 30). Therapeutic benefit has been reported by enhancing autophagy in ALS models with lithium treatment (31) and overexpressed TDP-43 models with rapamycin treatment (32). Conversely, there is a report showing that dietary restriction, but not rapamycin (an autophagy inducer), ameliorates the symptoms of mutant SOD1 transgenic mice (33) Therefore, the predominant involvement of autophagy in ALS pathogenesis is a matter of debate, This is in part due to the complex effects of pharmacological approaches other than autophagy suppression. To clarify the exact roles of protein quality control systems, the use of mouse genetic engineering approaches, especially those targeting motor neurons, is needed.

In the present study, we investigated the effect of disrupting proteasomes or autophagy only in motor neurons. To this end, we generated conditional knock-out (CKO) mice for Rpt3, a subunit of 19S particle that formed 26S proteasome, to disrupt the 26S proteasome, or Atg7, a crucial factor for the induction of autophagy, using the Cre-loxP system. Rpt3 is a subunit of 26S proteasome of which mutations are reported in Parkinson disease patients (34), and knock-out of mice *Rpt3* gene results in early-embryonic lethality (35). We show here that motor neuron-specific disruption of Rpt3, but not Atg7, induced the ALS phenotype both behaviorally and pathologically in mice. Although both types of mice displayed accumulation of ubiquitin or ubiquitinated proteins, TDP-43 and FUS pathologies were observed only in Rpt3-CKO mice. Our work has suggested the predominant role for the UPS in ALS pathogenesis, which may be mediated by TDP-43 and/or FUS proteinopathy.

EXPERIMENTAL PROCEDURES

Transgenic Mice Generation

Floxed Rpt3 Mice—Using homologous recombination, a cassette containing a loxP site with a neomycin resistance gene (Neo) flanked by flippase recognition target (FRT) sites (36) and a loxP site were inserted into introns 7 and 10, respectively, of the *Rpt3* gene (GenBank™ ID 23996) in the mouse C57BL/6N ES cell line RENKA (37) by electroporation. After ES cell selection, 5–10 positive transgenic ES cells were injected per 8-cell-stage embryo mice. After overnight culture, the ES cell-containing embryos that developed to the blastocyst stage were transplanted into the uterus of pseudo-pregnant ICR females. Germline-transmitted chimeric males were crossed with C57BL/6N females for the floxed Rpt3 mice to generate heterozygotes. After removing the neomycin resistance gene with the FLP-FRT system by crossing with FLP66 mice that express flippase (36), Rpt3+/flox intercrosses were done to establish homozygous floxed Rpt3 mice (Rpt3flox/flox) at apparent Mendelian frequencies. Rpt3flox/flox mice were phenotypically normal. Rpt3flox/flox mice were used after eight generations for this experiment. To selectively knock out Rpt3 activity in motor neurons, Rpt3delta/flox mice were crossed with VAChT-Cre.Fast mice (38) with the Rpt3+/flox allele to obtain the mutant mice. All studies were performed in accordance with the Guideline for Animal Studies of the Kyoto University and the National Institutes of Health. The committee of animal handling of Kyoto University and Juntendo University also approved the experimental procedures used.

Conditional VAChT-Rpt3 KO Mice—Rpt3delta/+; CAG-Cre+ mice were generated by crossing Rpt3flox/flox mice with CAG-Cre mice (39). After removing CAG-Cre by crossing with WT mice, Rpt3delta/+ mice were mated with Rpt3flox/flox mice to generate Rpt3delta/flox mice. Rpt3delta/flox mice were crossed with Rpt3+/flox; VAChT-Cre.Fast+ mice to produce Rpt3delta/flox; VAChT-Cre.Fast+ as mutant mice and Rpt3delta/+; VAChT-Cre.Fast+ mice as controls. Female mutant and control mice were used ($n = 8$). There were no differences in the results between male and female mutant mice. All genotyping was performed with PCR using DNA from tail biopsies.

Conditional VAChT-Atg7 KO Mice—Floxed Atg7 mice are described elsewhere (40). Atg7flox/flox mice were crossed with Atg7+/flox; VAChT-Cre.Fast+ mice to produce Atg7flox/flox; VAChT-Cre.Fast+ (Atg7-CKO) as the mutant mice and Atg7+/flox; VAChT-Cre.Fast+ mice as controls (Atg+control).

PCR Genotyping—Tails were lysed with 0.5% SDS and 100 mg/ml proteinase K. DNA was extracted from lysates with phenol/chloroform 1:1 (v/v), precipitated with isopropanol, and dissolved in 10 mM Tris-HCl, pH 7.5/1 mM EDTA. Genotyping

for the *Rpt3* flox allele was carried out with primers Rpt3 fl-for and Rpt3 fl-rev. Genotyping for the Rpt3 delta allele was carried out with primer Rpt3 del-rev (the forward primer used was the Rpt3 fl-for primer). PCR conditions were 94 °C for 5 min, and then 30 cycles of 94 °C for 30 s, 55 °C for 30 s, and 74 °C for 1 min on a thermal cycler. The presence of a 330-bp band is indicative of the wild-type allele, whereas the presence of a 390-bp band is specific for the *Rpt3* flox allele in Rpt3 flox allele detection PCR. The presence of a 360-bp band is specific for the *Rpt3* delta allele instead of a 1800-bp wild-type allele (the 1800-bp band is not detected with this PCR method time) in Rpt3 delta allele detection PCR. Genotyping for the *Cre* allele, which was included in CAG-Cre and VAChT-Cre.Fast mice, was carried out with primers Cre-for and Cre-rev. PCR conditions were 95 °C for 3 min, and then 30 cycles of 95 °C for 30 s, 60 °C for 30 s, and 72 °C for 30 s followed by an extension of 72 °C for 2 min on a thermal cycler. The presence of a 303-bp band is indicative of the *Cre* transgene. Genotyping for the *Flp* allele was carried out with primers Flp-for and Flp-rev. PCR conditions were 94 °C for 5 min, and then 30 cycles of 94 °C for 30 s, 58 °C for 30 s, and 72 °C for 1 min on a thermal cycler. The presence of a 480-bp band is indicative of the *Flp* transgene. Products of the reaction were analyzed by electrophoresis in a 2% agarose gel. Genotyping for the *Atg7* flox allele was carried out with primers Hind-Fw and 96–121c. PCR conditions were 94 °C for 5 min, and then 30 cycles of 98 °C for 20 s, 68 °C for 3 min, and 72 °C for 10 min on a thermal cycler. The presence of a 4.4-Kbp band is indicative of the *Atg7* flox allele, whereas the presence of a 2.2-kbp band is specific for the *Atg7* delta allele in Atg7 flox allele detection PCR. Products of the reaction were analyzed by electrophoresis in a 1% agarose gel.

Behavioral Analyses of Transgenic Mice—Using a rotarod device (47600, Ugo Basile), the retention time of mice on the rod running at an accelerating speed from 20 to 40 rounds per minutes (rpm) was measured with eight trials. If the mice stayed on the rod for 120 s, a time of 120 s was recorded. Grip strength of the mice was measured with a Grip strength meter (47106, Ugo Basile). Measurements were conducted five times per test with biweekly schedules by a researcher blind to the genotype and age of the mice. Body weights of the mice were measured weekly.

Histology

For the analysis of Rpt3-CKO mice, three mutant mice of 6, 12, and 40 weeks of age and three controls of the same ages were used; three mutant mice 2 years of age and three controls of the same age were used for Atg7-CKO mice. Mice were deeply anesthetized with pentobarbital (25 mg/kg, intraperitoneal) and fixed by cardiac perfusion with 4% paraformaldehyde (PA) buffered with 0.1 M phosphate buffer (pH 7.2) (PB) containing 4% sucrose for light microscopic immunohistochemistry and with 2% PA and 2% glutaraldehyde buffered with PB for electron microscopy. The spinal cords were removed from the mice and further fixed in the same fixatives for 2 h. The spinal cords were embedded in paraffin wax and cut into sections of 6-μm thickness according to standard protocols. For general morphological examination, we used hematoxylin (Harris) and eosin (H&E), Kluver-Barrera's staining, and Nissl staining.

For immunohistochemistry, first, endogenous peroxidase activity was quenched by incubation with 0.2% hydrogen peroxide in 0.1 M PB, pH 7.3 containing 0.2% Triton X-100 for 5 min at 37 °C. After antigen retrieval by heat/microwaving (5 min in 10 mM sodium citrate buffer, pH 6.0; except for ubiquitin), the sections were incubated with primary antibody (listed in supplemental Table S1) overnight at 4 °C. Bound antibodies were detected with the appropriate Vectastain Elite ABC kit (Vector Laboratories, Burlingame, CA) with tetrahydrochloride as the chromogen and observed under an Olympus BX-51 microscope (Olympus Corporation, Tokyo, Japan).

For double immunofluorescence staining, primary antibodies were visualized with Alexa Fluor 488-labeled goat anti-rabbit IgG (1:200, Molecular Probes, Eugene, OR) and Cy5-labeled goat anti-mouse IgG (1:100, Chemicon International, Temecula, CA). The slides were mounted with Vectashield with DAPI (Vector Laboratories) and observed under a Keyence BZ-9000 microscope and camera (Keyence Corporation, Osaka, Japan). We assessed the staining specificity by replacing the primary antibodies with an appropriate amount of non-immune rabbit serum or phosphate-buffered saline solution containing 3% bovine serum albumin. No deposits of reaction products were seen in these sections. For Atg7-CKO mice, the fixed samples were processed for paraffin embedding, cut into 5-μm sections with a microtome (RM2245; Leica, Germany), and immunostained according to the method described previously (41) with primary antibodies listed in supplemental Table S1. For Nbr1 and Atg7 staining, deparaffinized sections were autoclaved for 20 min in 10 mM Na-citrate buffer (pH 6.1) before incubation with rabbit anti-Nbr1 antibody.

Electron Microscopy

The fixed samples were cut into slices less than 1 mm, postfixed with 2% OsO_4 buffered with 0.1 M PB (pH 7.2), block-stained in 1% aqueous solution of uranyl acetate, dehydrated in a graded series of alcohols, and embedded in Epon 812 (TAAB). After confirming that semi-thin sections from the Epon-embedded blocks of spinal cords contained the ventral horn, silver-colored sections were cut with an ultramicrotome (Ultracut UC6; Leica microsystems). The ultrathin sections were then stained with uranyl acetate and lead citrate and observed with an electron microscope (HT7700; Hitachi).

Statistical Analysis

Two-group data analysis was performed using the two-tailed unpaired Student's *t* test with unequal variance. For data analysis of more than two groups, the significance of differences among test values was determined with the two-tailed multiple *t* test with Bonferroni correction following ANOVA (6 comparisons in 4 groups or 15 comparisons in 6 groups). Statistical significance is shown in each figure as appropriate.

RESULTS

Generation of Spinal Motor Neuron-specific Rpt3 Conditional Knock-out Mice—A floxed *Rpt3* construct was generated in which exons 7–10, encoding the majority of the conserved ATPase domain (42), were flanked by loxP sites and replaced with a neomycin resistance gene (Neo) that was adjoined by

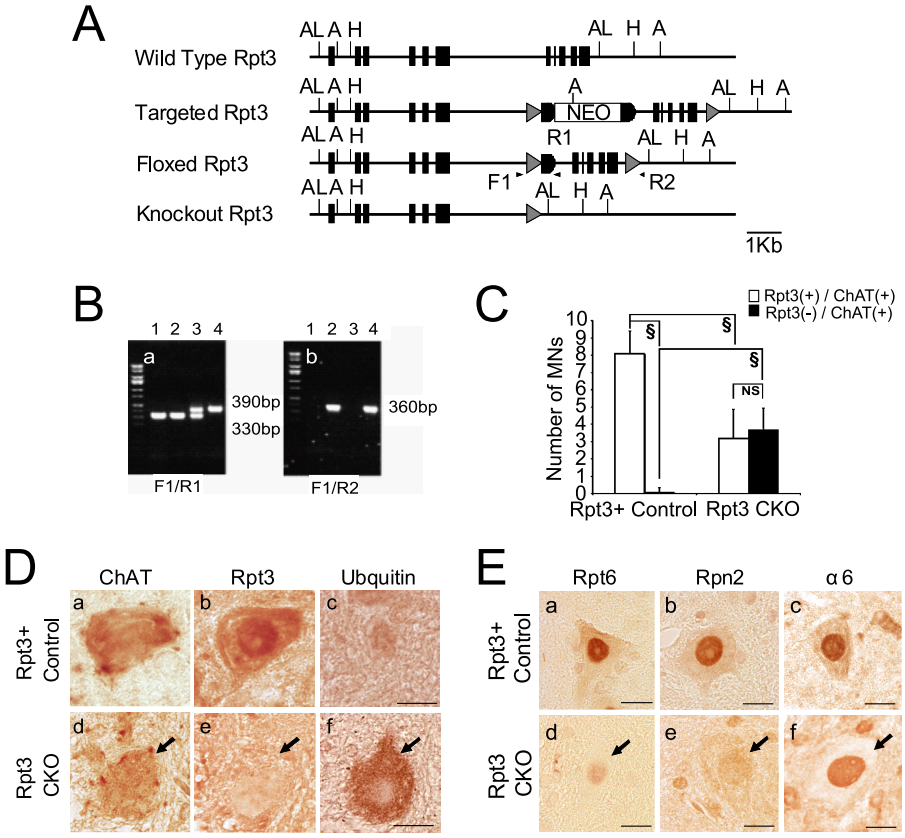

FIGURE 1. **Generation of Rpt3 conditional knock-out mice, Rpt3 delta/flox; VAChT-Cre.Fast+ (Rpt3-CKO), and influence on expression of proteasome subunits.** *A*, schematic diagram of the Rpt3flox construct. Cre removes the region of the *Rpt3* gene that encodes exons 7–10 (*black boxes*), which are flanked by loxP (*triangles*). The neomycin resistance gene (*white box*) between FRT (*closed half-circles*) was already removed by crossingFLP66 mice with Rpt3 floxed mice. *F1*, Rpt3 fl-for primer; *R1*, Rpt3 fl-rev primer; *R2*, Rpt3 del-rev primer; *A*, AatI; *AL*, ApaLI; *H*, HindIII. *B*, genotyping of floxed Rpt3 mice and Rpt3 delta mice with PCR. Rpt3+/+ (WT) mice (*1*), Rpt3 delta/+ mice (*2*), Rpt3+/flox mice (*3*), and Rpt3 delta/flox mice (*4*) are detected with PCR using tail DNA. *Left*, flox detection PCR; *right*, delta detection PCR. *C*, graphic representation of quantitative analysis of serial sections immunostained for Rpt3 and ChAT from control and Rpt3-CKO mice at 6 weeks of age. The number of ChAT-positive motor neurons with decreased Rpt3 immunoreactivity is significantly higher in Rpt3-CKO mice than in controls ($n = 3$, §, $p < 0.01$). *NS* indicates not significant. *D*, immunohistochemistry for ChAT, Rpt3, and ubiquitin in serial sections from the spinal cord of Rpt3-CKO mice (*d–f*) and control littermates (*a–c*). Representative image of ChAT-positive spinal motor neurons in Rpt3-CKO mice, showing that Rpt3-negative neurons show ubiquitin accumulation in the cytoplasm (*arrows*). Scale bars, 10 μm. *E*, immunohistochemistry for Rpt6 (*a* and *d*), Rpn2 (*b* and *e*), and α6 (*c* and *f*) on spinal cord sections from control and Rpt3-CKO mice. The motor neurons from Rpt3-CKO mice show no immunoreactivity for Rpt6 or Rpn2 in either the cytoplasm or the nuclei, or for α6 in the cytoplasm (*arrows*). Scale bars, 10 μm.

flippase recognition target (FRT) sites (36). The floxed *Rpt3* gene construct was inserted into the *Rpt3* gene in the mouse C57BL/6N ES cell line RENKA (37) by electroporation (Fig. 1*A*). To selectively ablate Rpt3 activity in spinal motor neurons, we crossed the floxed Rpt3 mice with VAChT-Cre.Fast mice, which express Cre in a spinal motor neuron-specific manner (38). Cre expression in VAChT-Cre.Fast mice is developmentally regulated, and ~50% of spinal motor neurons express Cre, the level of which reaches a maximum by 5 weeks of age (38). We generated $Rpt3^{delta/+}$; VAChT-Cre+ as a control mouse line, and $Rpt3^{delta/flox}$; VAChT-Cre+ (Rpt3-CKO) as the mutant mouse line (Fig. 1*B*). The number of Rpt3/choline acetyltransferase (ChAT) double-immunopositive spinal motor neurons in the mutant mice was reduced to approximately half of that in control mice at 6 weeks of age (Fig. 1*C*). Moreover, Rpt3-negative/ChAT-positive cells, comprising about 50% of the total spinal motor neurons, were observed exclusively in Rpt3-CKO mice, indicating that Rpt3 expression was deficient in about half of the spinal motor neurons in a Cre-dependent manner (Fig. 1*C*). Immunohistochemistry using serial spinal cord sections revealed that Rpt3 was effectively depleted in the ChAT-positive motor neurons (Fig. 1*D*, *arrows*). In agreement with this finding, ubiquitin immunoreactivity was increased in the cytoplasm of these cells, validating the severe impairment of the UPS (Fig. 1*D*). Moreover, we investigated the 26S proteasome subunits in Rpt3-CKO mice at 6 weeks of age, including Rpt6, a 19S base proteasome subunit connected directly to Rpt3 (43), Rpn2, a subunit required for 19S particle formation, and α6, a 20S proteasome subunit. We confirmed the reduction of immunoreactivity for Rpt6 and Rpn2 in the nuclei and cytosol only in Rpt3-CKO mice, strongly suggesting that the 19S particle was disassembled in Rpt3-deficient motor neuronsneurons (Fig. 1*E*).

Behavioral Abnormalities in Rpt3-CKO Mice—Behavioral analysis of Rpt3-CKO mice revealed that motor neuron-specific proteasome inhibition caused a progressive motor deterioration. Rpt3-CKO mice displayed significantly decreased rotarod performance after 26 weeks of age (Fig. 2*A*). This performance (16–36 weeks of age) and remained stable after 36 weeks of age. Body weight (Fig. 2*B*) and grip strength (Fig. 2*C*) were significantly reduced in Rpt3-CKO mice compared with controls. Onset of the ALS phenotype was observed at 10 weeks

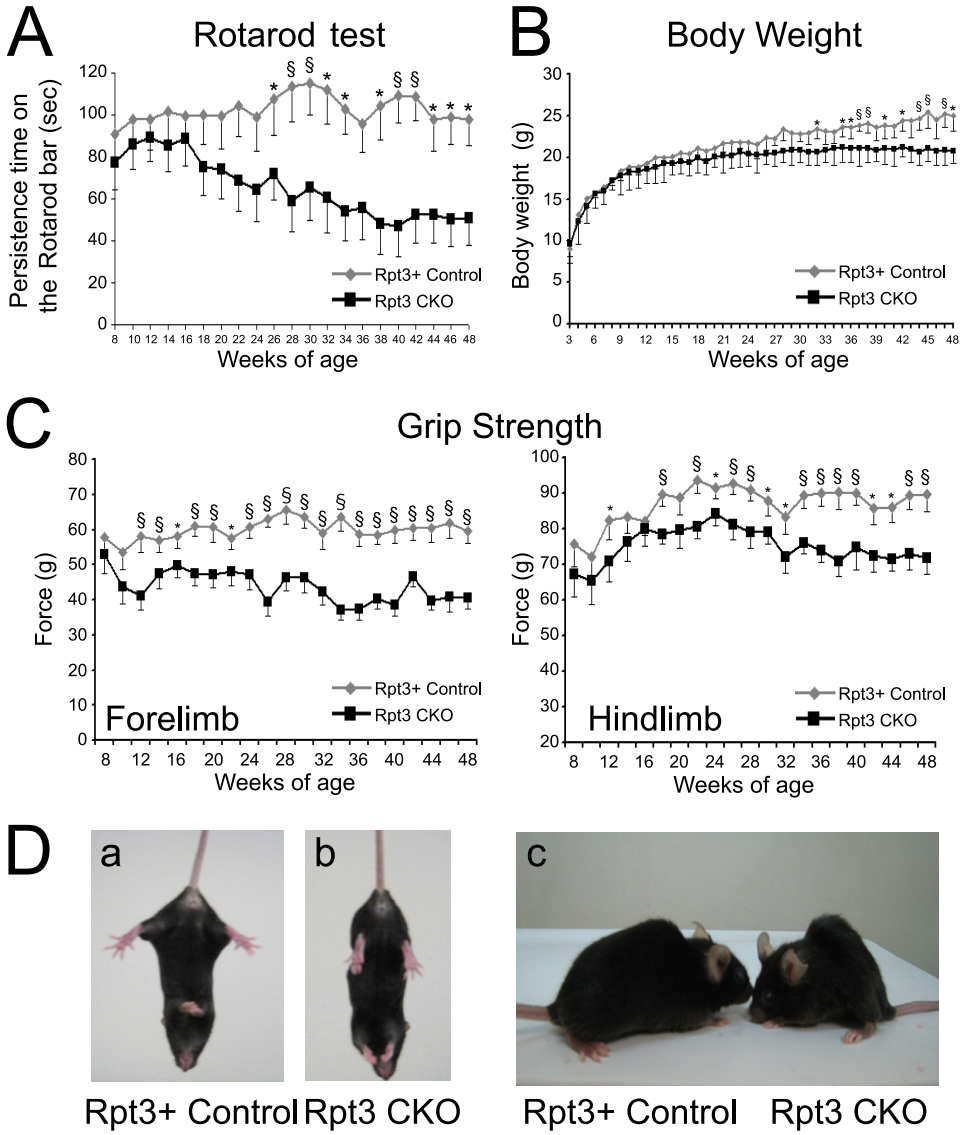

FIGURE 2. **Motor dysfunction in Rpt3-CKO mice.** Motor performance of Rpt3-CKO mice was evaluated by measuring rotarod retention time (*A*), body weight (*B*), grip strength (*C*), and tail suspension (*D*). *A*, rotarod analysis indicates that the mean retention time on the moving rod progressively decreases after 16 weeks of age in Rpt3-CKO mice. The differences in retention time between Rpt3-CKO mice and control littermates are statistically significant at 26 weeks of age and later ($n = 8$, *, $p < 0.05$, §, $p < 0.01$). *B*, progressive reduction in body weight of Rpt3-CKO mice. The mean body weight of Rpt3-CKO mice is significantly lower than that of control mice after 36 weeks of age ($n = 8$, *, $p < 0.05$, §, $p < 0.01$). *C*, grip strengths of both forelimbs and hindlimbs are significantly weaker in Rpt3-CKO mice than those in control mice after 12 weeks of age ($n = 8$, *, $p < 0.05$, §, $p < 0.01$). *D*, representative photographs of a control and an Rpt3-CKO mouse at 35 weeks of age displaying an abnormal limb-clasping reflex during tail hanging in the Rpt3-CKO mouse (*b*) and normal clasping in the control littermate (*a*). Representative photo of a Rpt3-CKO mouse at the advanced stage, showing severe kyphosis caused by weakness of the paraspinal muscles (*c*).

of age when the mice displayed disturbed and tremulous hindlimb movement with tail suspension. Other measures showed obvious differences later than 20 weeks (Fig. 2*D*). At the advanced stage, mice presented with severely deformed spines, indicating weakness of the paraspinal muscles (Fig. 2*D*). Of note, no survival difference was observed between Rpt3-CKO and control mice until at least 48 weeks of age. There was no gender difference in our mice.

Replication of Pathological Features of ALS in Rpt3-CKO Mice—Immunohistochemical analysis using anti-ChAT antibody showed progressive loss of spinal motor neurons in Rpt3-CKO mice from 6 weeks of age (Fig. 3*A*). Abnormal motor neurons with eosinophilic cytoplasm were found in the mutant spinal cords at 12 weeks of age (Fig. 3*B*, *arrows*). Notably, chromatolytic neurons and basophilic inclusions were present at 12 weeks of age (Fig. 3*C*, *arrows*). These cytopathological findings resemble those observed in the spinal motor neurons of sporadic ALS patients (Fig. 3*C*, *c* and *d*).

Next, we investigated the presence of pathological hallmarks of sporadic ALS, including TDP-43 (3, 4), FUS (5, 6), optineurin (7), and ubiquilin 2 (44). As shown in Fig. 4, immunohistochemistry demonstrated aberrant staining patterns of these proteins, including mislocalization and inclusions of TDP-43 (Fig. 4*A*, *a–c*) and FUS (Fig. 4*A*, *e–g*), accumulation of optineurin (Fig. 4*A*, *i–k*), and ubiquilin 2 inclusions (Fig. 4*A*, *m–o*). As shown in supplemental Fig. S1, TDP-43 displayed various cytoplasmic distributions with occasional nuclear inclusions (supplemental Fig. S1*D*, *arrows*). Mislocalized TDP-43 or FUS showed diffuse distribution in the cytosol at 6 weeks of age (asymptomatic stage; Fig. 4*A*, *b* and *f*), whereas aggregate formation of TDP-43,

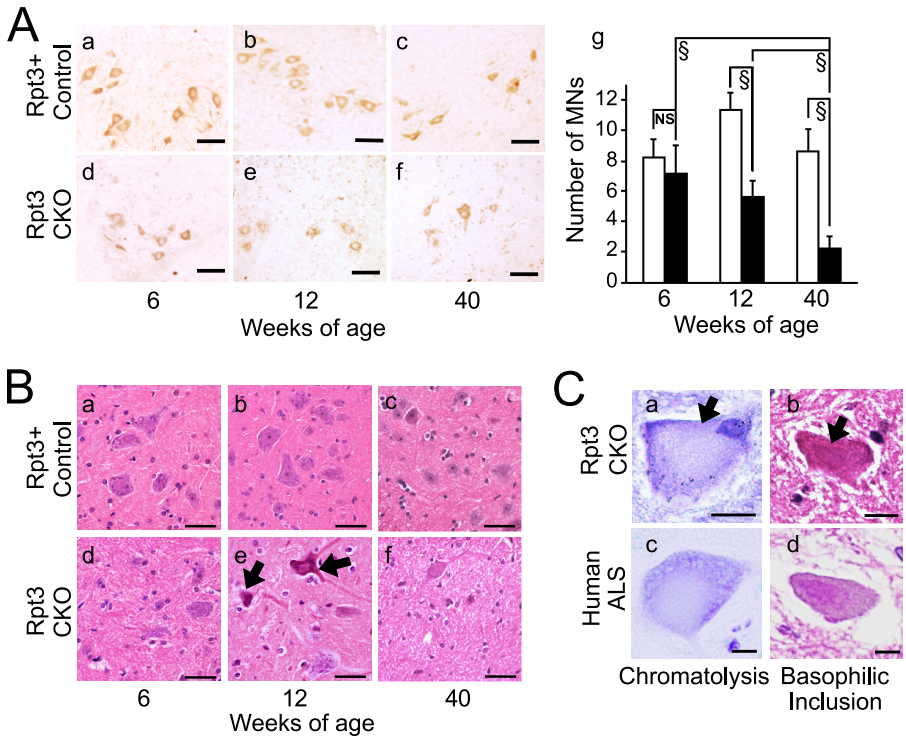

FIGURE 3. **Neuronal loss and cytopathology of the spinal motor neurons in Rpt3-CKO mice.** *A*, ChAT immunohistochemistry of spinal anterior horn cells from Rpt3-CKO mice (*d–f*) and control mice (*a–c*) at 6, 12, and 40 weeks of age. The number of motor neurons, indicated by ChAT-positive immunoreactivity, in Rpt3-CKO mice is significantly lower at 12 and 40 weeks of age than that of control mice (*g*)($n = 3$, §, $p < 0.01$). *NS* indicates not significant. *B*, H&E staining of anterior horns from control (*a–c*) and Rpt3-CKO mice (*d–f*). Rpt3-CKO mice (12 weeks) have abnormal motor neurons with eosinophilic substances in the cytosol (*arrows*). *C*, spinal motor neurons from Rpt3-CKO mice show chromatolysis and basophilic inclusions, resembling those in ALS patients. *a* and *c*, Nissl staining; *b* and *d*, H&E staining. Scale bars, 30 μm (*A*), 20 μm (*B*), and 10 μm (*C*).

FUS, or ubiquilin 2 was observed after 12 weeks of age when the mice were paralyzed (Fig. 4*A*, *c*, *g*, or *o*). Double immunofluorescence analysis demonstrated colocalization of TDP-43 with FUS (Fig. 4*B*, *a–c*) and ubiquilin 2 (Fig. 4*B*, *d–f*) within cytoplasmic inclusions. On the other hand, p62/SQSTM1, autophagy-specific substrate, was not detected in motor neurons and their surroundings in Rpt3-CKO mice at 12 weeks of age (data not shown). Quantification by counting cells with stronger staining of mislocalized than nuclear TDP-43 or *vice versa* revealed that the ratio of motor neurons with mislocalized to nuclear TDP-43 was maximal at 12 weeks of age (Fig. 4*C*). Interestingly, the ratio decreased at 40 weeks when motor neuron loss was most prominent (Fig. 4*C*), indicating that cytoplasmic TDP-43-positive motor neurons had disappeared.

Glial Activation in the Spinal Cord of Rpt3-CKO Mice—We next performed immunohistochemistry for glial cells in the spinal cord of Rpt3-CKO mice. In particular, we focused on astrocytes, because recent evidence shows that they play crucial roles not only in disease progression (45), but also in disease initiation (46). Glial fibrillary acidic protein (GFAP)-positive astrocytes were obviously detectable in the anterior horns of the spinal cords as early as 6 weeks (asymptomatic age; Fig. 5, *A*, *a*, *b*, *g*, *h*, and *Ca*). The robust astrocytosis persisted in the mutant spinal cords until 40 weeks of age (Fig. 5, *A*, *c–f*, *i–l*, and *Ca*). On the other hand, many activated microglia, which express galectin-3/MAC-2 (47), were found near motor neurons at 12 weeks, but fewer were found at 40 weeks of age (Fig. 5, *B* and *Cb*). In control mice, marginally reactive astrocytes and MAC-2-positive activated microglia were observed until 40 weeks of age, and their distribution was not concentrated in anterior horns (Fig. 5, *A*--*C*).

Lack of Overt ALS Phenotype in Transgenic Mice with Defective Autophagy in Motor Neurons—We also investigated a role for autophagy in motor neurons in ALS pathogenesis, using a similar genetic engineering approach. We generated $Atg7^{flox/flox}$; VAChT-Cre.Fast+ (Atg7-CKO) mice by crossing floxed Atg7 mice (22) with VAChT-Cre.Fast mice (Fig. 6*A*). Surprisingly, Atg7-CKO mice developed normally and showed neither an apparent defect in motor performance nor motor neuron loss at least at 2 years of age (Fig. 6*B*, *a* and *b*). Moreover, Atg7 negative motor neurons containing inclusion bodies were detected at this old age, demonstrating that autophagy-deficient motor neurons survive for life (Fig. 6*B*, *c* and *d*). As shown in Fig. 6*C*, Atg7-CKO mice at 2 years of age showed marked staining of ubiquitin and ubiquilin 2 (Fig. 6*C*, *f* and *p*), which were also detected in Rpt3-CKO mice (Fig. 1, *Df*, Fig. 4, *N* and *O*). As expected, p62/SQSTM1 and Nbr1, autophagy-specific substrates (48, 49), also accumulated (Fig. 6*C*, *g* and *h*). Electron microscopy revealed that motor neurons in Atg7-CKO mice had inclusions (asterisks) in which amorphous structures that similar to previous reported (22) accumulated, and large inclusions were found at 2 years of age (Fig. 6*D*). On the other hand, Atg7-CKO mice showed no cytoplasmic mislocalization or aggregate formation of TDP-43, FUS, or optineurin (Fig. 6*C*, *m–p*).

DISCUSSION

In the present study, we provide compelling evidence that a motor neuron-specific defect in proteasomes, but not

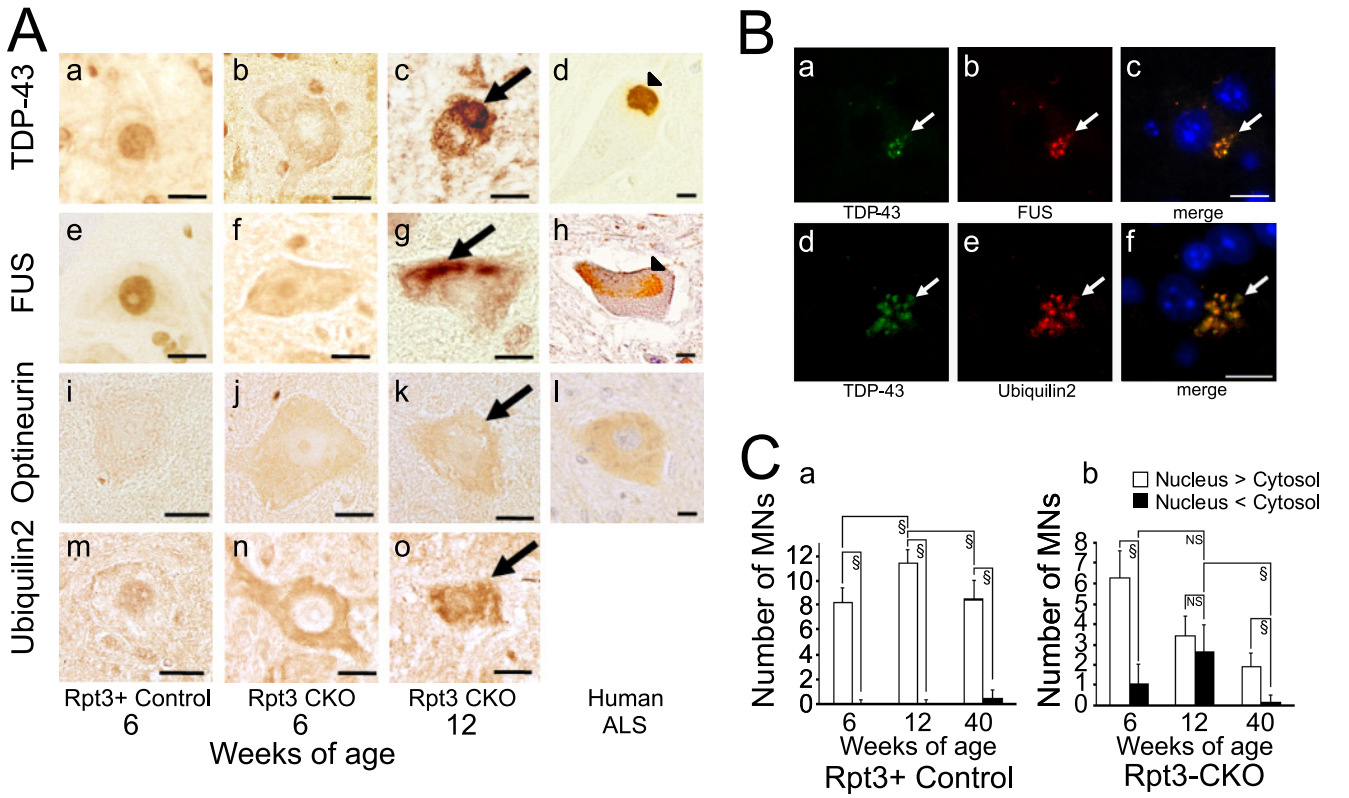

FIGURE 4. **Aberrant staining patterns of TDP-43, FUS, ubiquilin 2, and optineurin in the spinal motor neurons of Rpt3-CKO mice.** *A*, immunohistochemistry for TDP-43 (*a–c*), FUS (*e–g*), optineurin (*i–k*), and ubiquilin 2 (*m–o*) in spinal cords from Rpt3-CKO mice at 6 (*b*, *f*, *j*, *n*) and 12 (*c*, *g*, *k*, *o*) weeks of age and control mice at 6 weeks of age (*a*, *e*, *i*, *m*). Cytoplasmic mislocalization of TDP-43, FUS, and ubiquilin 2 and increased optineurin are observed in motor neurons from Rpt3-CKO mice as early as 6 weeks of age. Noticeable intracytoplasmic inclusions of TDP-43, FUS, and ubiquilin 2 (*arrows*) are recognizable at 12 weeks of age. Note that these inclusions resemble those in human ALS patients (*d*, *h*, *arrowheads*). *B*, double immunofluorescence investigations demonstrating co-localization of TDP-43 (*a*, *d*, *green*) with FUS (*b*, *red*) or ubiquilin 2 (*e*, *red*) in the intracytoplasmic inclusions of spinal motor neurons (*arrows*). Merged images are shown in *c* and *d*. Nuclei are stained with DAPI (*blue*). Scale bars, 10 mm. *C*, immunoreactivity to TDP-43 in the nucleus and the cytosol was compared, and the number of positive cells was counted under the microscope. A few motor neurons with nuclear exclusions were found in control mice (*a*). In contrast, the number of motor neurons in which the cytoplasm was more intensely stained with anti-TDP-43 antibody than the nucleus was significantly increased in 12-week-old Rpt3-CKO mice (*b*) ($n = 3$, §, $p < 0.01$).

autophagy, replicates ALS in mice. Our Rpt3-CKO mice express Cre in ~50% of spinal motor neurons (38). This population of motor neurons with defective proteasomes was found to produce an ALS-like phenotype. Immunohistochemistry validated the efficient disruption of 26S proteasomes in motor neurons, in which ubiquitin, Rpt6, Rpn2, and the α6 subunit of the 20S proteasome accumulated together with several hallmarks of ALS, including TDP-43, FUS, optineurin, and ubiquilin 2. Our data also suggest that protein quality control by proteasomes predominates in governing motor neuron survival compared with that by autophagy. Surprisingly, inhibition of autophagy in motor neurons was not as toxic as proteasome inhibition despite the robust increase in ubiquitinated substances.

Of note, TDP-43 proteinopathy was evident only in Rpt3-CKO mice, but not in Atg7-CKO mice. This result conflicts with the previous findings in a cell culture study in which TDP-43 was shown to be degraded through both autophagy and proteasomes (30, 50). Indeed, inhibition of either prolonged the half-life of TDP-43 in the pulse-chase study. However, immunofluorescence analysis demonstrated that overt cytosolic aggregates of TDP-43 are induced only in the presence of lactacystin, a specific proteasome inhibitor, but not 3-MA alone, an autophagy inhibitor (30). Therefore, the proteasome may be a dominant site for TDP-43 degradation, especially misfolded TDP-43, whereas autophagy may partially compensate to eliminate TDP-43. The population of motor neurons with mislocalized TDP-43 gradually increased until 12 weeks of age. Of note, TDP-43 mislocalization and Rpt3 downregulation were not concurrent in our mice. Rpt3 reduction became obvious as early as 5 weeks of age, 7 weeks before the overt accumulation of TDP-43, consistent with the idea that TDP-43 proteinopathy is caused by proteasome inhibition (Fig. 7).

Despite the clear difference in TDP-43 pathology between proteasome inhibition and autophagy disruption, the exact molecular machineries involved in proteasome-specific cascades are unclear. Both systems have been implicated in several neurodegenerative diseases, including Huntington disease, Parkinson disease, and Alzheimer disease, as well as ALS. Protein degradation via proteasomes is regulated by the substrate-specific ubiquitin-proteasome pathway, the impairment of which induces diverse toxic cascades via accumulation of misfolded or dysfunctional proteins in the cytosol or other organelles such as the endoplasmic reticulum or mitochondria (51). On the other hand, autophagy is chiefly a bulk degradation system, which serves for quality control of organelles such as mitochondria as well as various membranous or cytoplasmic proteins (52). Familial ALS-linked mutant SOD1 proteins are

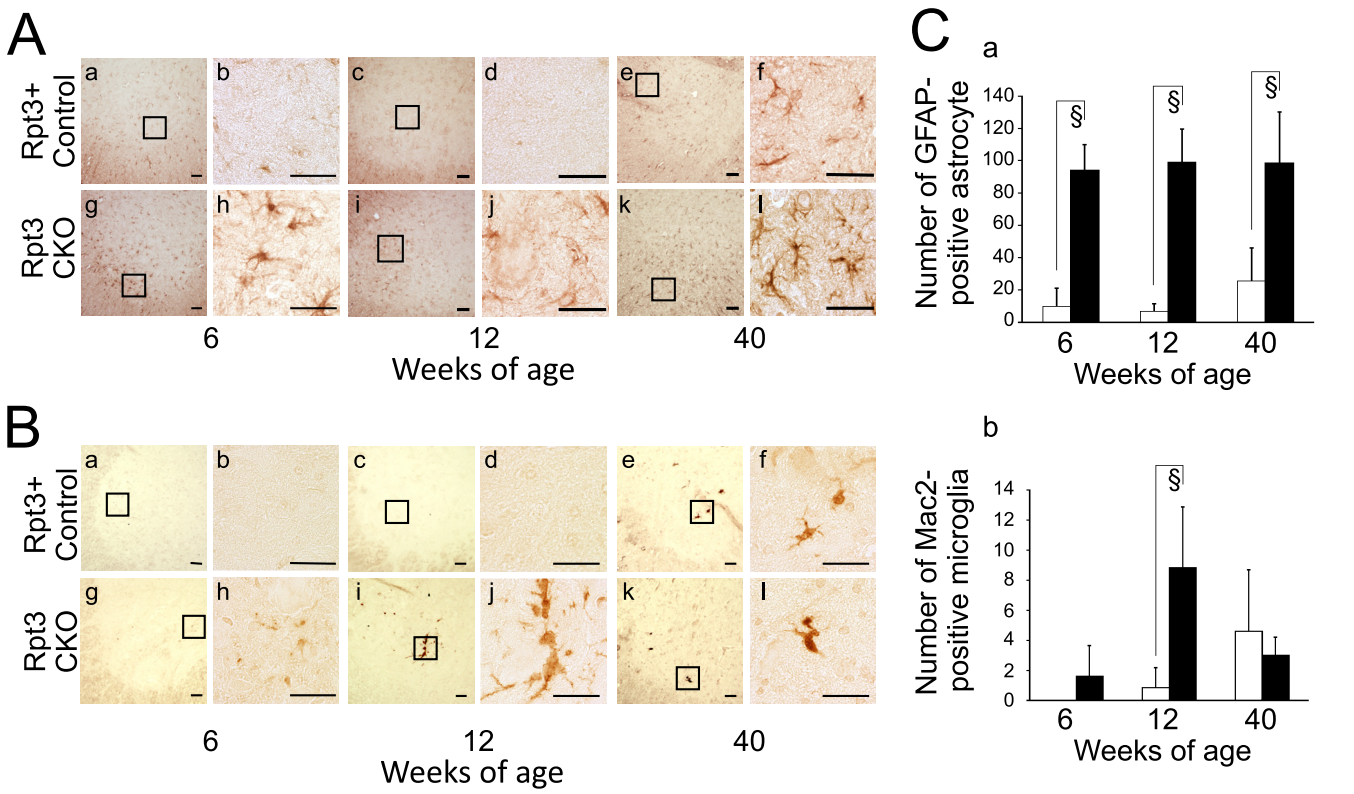

FIGURE 5. **Glial activation in spinal anterior horns of Rpt3-CKO mice.** *A*, immunohistochemistry for GFAP in spinal anterior horns of control (*a–f*) and Rpt3-CKO mice (*g–l*), showing an increase in size and number of reactive astrocytes in anterior horns at 6 weeks of age, which further progressed along with the disease progression (*a–f*). Control mice demonstrate apparently low levels of astrogliosis (*g–l*). Scale bars, 10 μm. *B*, immunohistochemistry for MAC-2 in the spinal anterior horns of control (*a–f*) and Rpt3-CKO mice (*g–l*). MAC-2-positive reactive microglia with amoeboid morphology proliferate in the anterior horn at 12 weeks of age, but not at 6 weeks of age. Note that MAC-2-positive microglia have regressed by 40 weeks of age in Rpt3-CKO mice (*k* and *l*). Scale bars, 10 μm. *C*, quantitative evaluation of astrocytosis (*a*) and microgliosis (*b*). Number of GFAP-positive reactive astrocytes increases significantly in the spinal anterior horns of Rpt3-CKO mice from 6 weeks (*upper*), and remains high until 40 weeks (*a*). MAC-2-positive microglia showed a later increase, which is statistically significant at 12 weeks of age (*b*) ($n = 3$, §, $p < 0.01$).

degraded by autophagy as well as by proteasomes (24, 29). In mutant SOD1 Tg mice, the mammalian target of rapamycin-dependent autophagic pathway is activated until the early symptomatic period as evidenced by an increase in microtubule-associated protein 1 light chain 3-II (LC3-II) and autophagic vacuoles. However, autophagic impairment is shown at the end stage by the accumulation of p62 or autophagic vacuoles. These findings suggest the involvement of autophagy machinery in the pathogenesis of ALS, especially in mutant SOD1-linked ALS (53). Nevertheless, our results documenting a primary role for proteasomes in the development of ALS pathology indicate that proteasomes should be highlighted as a direct therapeutic target, rather than autophagy system.

The role of proteasome inhibition in cell death is not established in cultured cells. For instance, selective disruption of the specific 19S proteasome subunits Rpn10, Rpn11, and Rpt5 induces the accumulation of ubiquitinated inclusions, but does not cause cell death in cultured neurons (54) On the contrary, reports have shown that inhibition of 20S particle activity leads to apoptotic cell death accompanied by the accumulation of ubiquitinated proteins (55–58). For the first time, we have provided evidence that proteasome impairment in motor neurons directly links to pathogenesis of ALS, based on the successful *in vivo* elimination of proteasome components in mice. It should be noted that the proteasome disruption in half of spinal motor neurons lead to motor neurons loss by 75%. This suggests the participation of non-cell autonomous machineries such as glial involvement or propagation of unidentified toxic substrates from the dead motor neurons.

Pathological findings in our mice included hallmarks of sporadic ALS, including chromatolysis, eosinophilic round hyaline inclusions, skein-like inclusions, and basophilic inclusions. Moreover, these inclusions were immunoreactive for TDP-43, FUS, optineurin, and ubiquilin 2. In addition, TDP-43 mislocalization preceded the aberrant staining of FUS in our mice. A previous report documented that TDP-43 interacts with FUS to induce the expression of histone deacetylase 6 in the nucleus, and the carboxyl terminus of TDP-43 is reportedly required for this interaction (59). Therefore, the carboxyl fragments of TDP-43, subsequent to its aberrant cytoplasmic mislocalization, may promote the recruitment of FUS during the process to form inclusions. Otherwise, a detrimental environment due to proteasome inhibition may induce stress granules, possibly providing the opportunity for assembly of these stress granule proteins, regardless of the carboxyl fragments of TDP-43 (60).

The different temporal profiles between astrocytosis and microgliosis are also interesting in interpreting the pathogenesis of ALS related to proteasome dysfunction. Active astrocytes proliferated at 6 weeks of age, whereas microgliosis was most robust at 12 weeks when the loss of motor neurons was evident (Fig. 7). Although the exact role of these types of gliosis remains unclear, our finding indicates that astrocytes serve as early

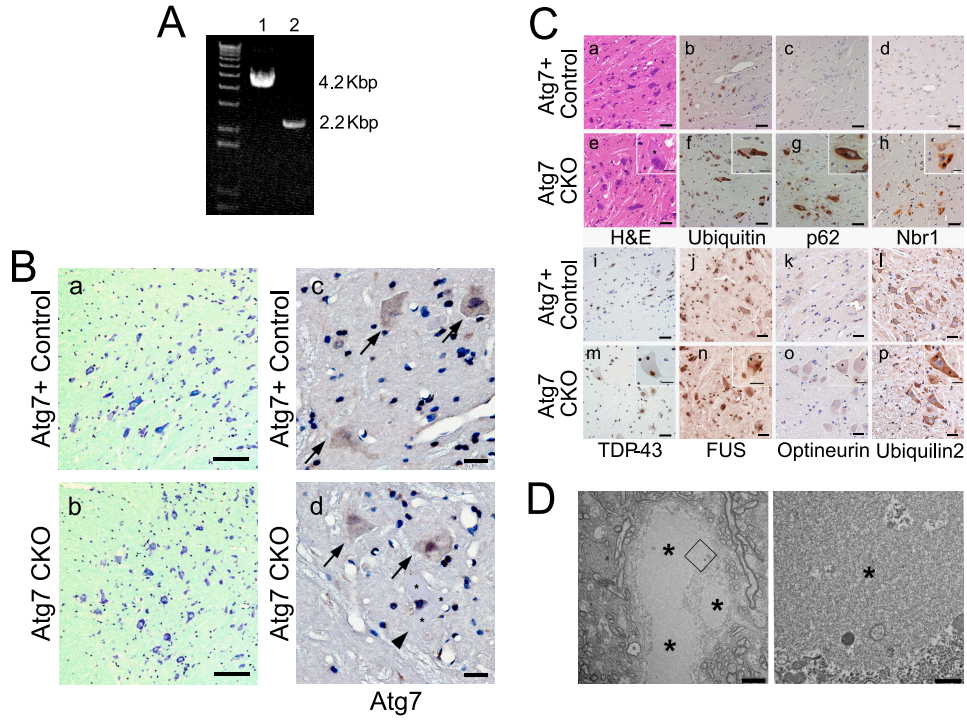

FIGURE 6. **Histochemical analysis of mice with defective autophagy in motor neurons (Atg7-CKO).** *A*, genotyping of transgenic mice for floxed and delta Atg7 with PCR. Atg7 flox allele (*1*) and Atg7 delta allele (*2*) were detected agarose gel electrophoresis showing Cre-dependent deletion of loxP-franked region for Atg7 in Atg7-CKO mice (*2*) compared with Atg+ control (*1*). *B*, Nissl staining of anterior horns from control (*a*) and Atg7-CKO mice (*b*). Atg7-CKO mice have no motor neurons loss. Immunohistochemistry for Atg7 on spinal cord sections of control and Atg7-CKO mice (*c* and *d*). Atg7-negative neurons (*arrowhead*) showed inclusions (*asterisks*) instead of Atg7-positive neurons (*arrow*). Scale bars, 40 μm (*a* and *b*), 10 μm (*c* and *d*), *C*, H&E staining (*a* and *e*) and immunohistochemistry for ubiquitin (*b*, *f*), p62 (*c*, *g*), Nbr1 (*d*, *h*), TDP-43 (*i*, *m*), FUS (*j*, *o*), optineurin (*k*, *p*), and ubiquilin 2 (*l*, *q*) in spinal anterior horns from Atg7+control (*a–d*, *i–l*) and Atg7-CKO (*e–h*, *m–p*) mice. Motor neurons in Atg7-CKO mice showed marked accumulation of p62, ubiquitin, Nbr1, and ubiquilin 2 without cytoplasmic mislocalization or aggregate formation of TDP-43, FUS, or optineurin (*asterisks*). Scale bars, 20 μm (low magnification), 10 μm (high magnification). *D*, electron microscopy imaging of large inclusions (*asterisks*) in which amorphous structures accumulated in an Atg7-CKO mouse at 2 years of age. Scale bars, 5 μm (*left*), 1 μm (*right*).

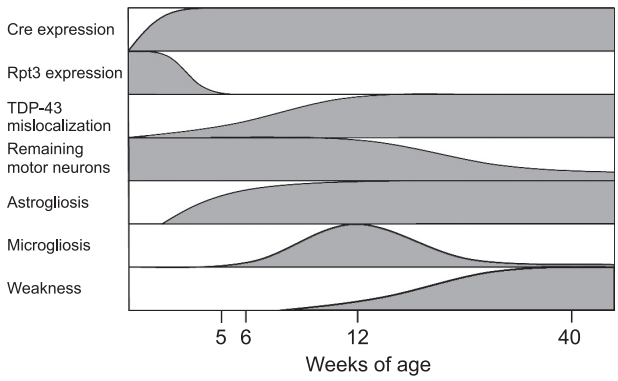

FIGURE 7. **Temporal profiles demonstrating the ALS-like phenotypes with proteasome inhibition and TDP-43 mislocalization.** Rpt3 down-regulation is induced by excision of the Rpt3 gene by Cre until 6 weeks of age. The population of motor neurons with TDP-43 mislocalization gradually increased after Rpt3 down-regulation. Astrogliosis precedes paralytic symptoms, motor neuron loss, and microgliosis.

modulators or responders to the development of ALS, not only of the progression (45, 61). Moreover, considering that proteasome impairment preceded the sequential activation of astrocytes followed by microglia, signaling molecules released from motor neurons may be crucially involved in the glial activation in ALS. The identification of such molecules may expand our understanding of ALS.

In conclusion, we have shown that dysfunction of 26S proteasomes in motor neurons is sufficient to induce cytopathological phenotypes of ALS. Thus, UPS dysfunction may primarily contribute to the pathogenesis of sporadic ALS, and preservation and/or activation of UPS may represent an effective therapeutic approach to overcome ALS.

Acknowledgments—We thank S. Murata for antibodies, R. Natsume, M. Iwama, N. Tada, and T. Iwasato for mice, and R. Wate for helpful support in producing the artwork. CAG-Cre mice were developed and provided by K. Sakai and J. Miyazaki, and FLP66 mice were from T. Takeuchi and M. Mishina.

REFERENCES

1. Rosen, D. R., Siddique, T., Patterson, D., Figlewicz, D. A., Sapp, P., Hentati, A., Donaldson, D., Goto, J., O'Regan, J. P., and Deng, H. X. (1993) Mutations in Cu/Zn superoxide dismutase gene are associated with familial amyotrophic lateral sclerosis. *Nature* **362,** 59–62
2. Hadano, S., Hand, C. K., Osuga, H., Yanagisawa, Y., Otomo, A., Devon, R. S., Miyamoto, N., Showguchi-Miyata, J., Okada, Y., Singaraja, R., Figlewicz, D. A., Kwiatkowski, T., Hosler, B. A., Sagie, T., Skaug, J., Nasir, J., Brown, R. H., Jr., Scherer, S. W., Rouleau, G. A., Hayden, M. R., and Ikeda, J. E. (2001) A gene encoding a putative GTPase regulator is mutated in familial amyotrophic lateral sclerosis 2. *Nat. Genet.* **29,** 166–173
3. Arai, T., Hasegawa, M., Akiyama, H., Ikeda, K., Nonaka, T., Mori, H., Mann, D., Tsuchiya, K., Yoshida, M., Hashizume, Y., and Oda, T. (2006) TDP-43 is a component of ubiquitin-positive tau-negative inclusions in frontotemporal lobar degeneration and amyotrophic lateral sclerosis. *Biochem. Biophys. Res. Commun.* **351,** 602–611
4. Neumann, M., Sampathu, D. M., Kwong, L. K., Truax, A. C., Micsenyi, M. C., Chou, T. T., Bruce, J., Schuck, T., Grossman, M., Clark, C. M.,

McCluskey, L. F., Miller, B. L., Masliah, E., Mackenzie, I. R., Feldman, H., Feiden, W., Kretzschmar, H. A., Trojanowski, J. Q., and Lee, V. M. (2006) Ubiquitinated TDP-43 in frontotemporal lobar degeneration and amyotrophic lateral sclerosis. *Science* **314,** 130–133

5. Kwiatkowski, T. J., Jr., Bosco, D. A., Leclerc, A. L., Tamrazian, E., Vanderburg, C. R., Russ, C., Davis, A., Gilchrist, J., Kasarskis, E. J., Munsat, T., Valdmanis, P., Rouleau, G. A., Hosler, B. A., Cortelli, P., de Jong, P. J., Yoshinaga, Y., Haines, J. L., Pericak-Vance, M. A., Yan, J., Ticozzi, N., Siddique, T., McKenna-Yasek, D., Sapp, P. C., Horvitz, H. R., Landers, J. E., and Brown, R. H., Jr. (2009) Mutations in the FUS/TLS gene on chromosome 16 cause familial amyotrophic lateral sclerosis. *Science* **323,** 1205–1208
6. Vance, C., Rogelj, B., Hortobágyi, T., De Vos, K. J., Nishimura, A. L., Sreedharan, J., Hu, X., Smith, B., Ruddy, D., Wright, P., Ganesalingam, J., Williams, K. L., Tripathi, V., Al-Saraj, S., Al-Chalabi, A., Leigh, P. N., Blair, I. P., Nicholson, G., de Belleroche, J., Gallo, J. M., Miller, C. C., and Shaw, C. E. (2009) Mutations in FUS, an RNA processing protein, cause familial amyotrophic lateral sclerosis type 6. *Science* **323,** 1208–1211
7. Maruyama, H., Morino, H., Ito, H., Izumi, Y., Kato, H., Watanabe, Y., Kinoshita, Y., Kamada, M., Nodera, H., Suzuki, H., Komure, O., Matsuura, S., Kobatake, K., Morimoto, N., Abe, K., Suzuki, N., Aoki, M., Kawata, A., Hirai, T., Kato, T., Ogasawara, K., Hirano, A., Takumi, T., Kusaka, H., Hagiwara, K., Kaji, R., and Kawakami, H. (2010) Mutations of optineurin in amyotrophic lateral sclerosis. *Nature* **465,** 223–226
8. Da Cruz, S., and Cleveland, D. (2011) Understanding the role of TDP-43 and FUS/TLS in ALS and beyond. *Curr. Opin. Neurobiol.* **21,** 904–919
9. Mizusawa, H., Matsumoto, S., Yen, S. H., Hirano, A., Rojas-Corona, R. R., and Donnenfeld, H. (1989) Focal accumulation of phosphorylated neurofilaments within anterior horn cell in familial amyotrophic lateral sclerosis. *Acta Neuropathol.* **79,** 37–43
10. Okamoto, K., Hirai, S., Ishiguro, K., Kawarabayashi, T., and Takatama, M. (1991) Light and electron microscopic and immunohistochemical observations of the Onuf's nucleus of amyotrophic lateral sclerosis. *Acta Neuropathol.* **81,** 610–614
11. Taylor, J. P., Hardy, J., and Fischbeck, K. H. (2002) Toxic proteins in neurodegenerative disease. *Science* **296,** 1991–1995
12. Wong, E., and Cuervo, A. M. (2010) Autophagy gone awry in neurodegenerative diseases. *Nat. Neurosci.* **13,** 805–811
13. Glickman, M. H., and Ciechanover, A. (2002) The ubiquitin-proteasome proteolytic pathway: destruction for the sake of construction. *Physiol. Rev.* **82,** 373–428
14. Welchman, R. L., Gordon, C., and Mayer, R. J. (2005) Ubiquitin and ubiquitin-like proteins as multifunctional signals. *Nat. Rev. Mol. Cell Biol.* **6,** 599–609
15. Kitada, T., Asakawa, S., Hattori, N., Matsumine, H., Yamamura, Y., Minoshima, S., Yokochi, M., Mizuno, Y., and Shimizu, N. (1998) Mutations in the parkin gene cause autosomal recessive juvenile parkinsonism. *Nature* **392,** 605–608
16. Leroy, E., Boyer, R., Auburger, G., Leube, B., Ulm, G., Mezey, E., Harta, G., Brownstein, M. J., Jonnalagada, S., Chernova, T., Dehejia, A., Lavedan, C., Gasser, T., Steinbach, P. J., Wilkinson, K. D., and Polymeropoulos, M. H. (1998) The ubiquitin pathway in Parkinson's disease. *Nature* **395,** 451–452
17. Matsui, H., Ito, H., Taniguchi, Y., Inoue, H., Takeda, S., and Takahashi, R. (2010) Proteasome inhibition in medaka brain induces the features of Parkinson's disease. *J. Neurochem.* **115,** 178–187
18. Wang, H. Q., Imai, Y., Inoue, H., Kataoka, A., Iita, S., Nukina, N., and Takahashi, R. (2008) Pael-R transgenic mice crossed with parkin deficient mice displayed progressive and selective catecholaminergic neuronal loss. *J. Neurochem.* **107,** 171–185
19. Bedford, L., Hay, D., Devoy, A., Paine, S., Powe, D. G., Seth, R., Gray, T., Topham, I., Fone, K., Rezvani, N., Mee, M., Soane, T., Layfield, R., Sheppard, P. W., Ebendal, T., Usoskin, D., Lowe, J., and Mayer, R. J. (2008) Depletion of 26S proteasomes in mouse brain neurons causes neurodegeneration and Lewy-like inclusions resembling human pale bodies. *J. Neurosci.* **28,** 8189–8198
20. Harris, H., and Rubinsztein, D. C. (2012) Control of autophagy as a therapy for neurodegenerative disease. *Nat. Rev. Neurol.* **8,** 108–117
21. Tsvetkov, A. S., Miller, J., Arrasate, M., Wong, J. S., Pleiss, M. A., and Finkbeiner, S. (2010) A small-molecule scaffold induces autophagy in primary neurons and protects against toxicity in a Huntington disease model. *Proc. Natl. Acad. Sci. U.S.A.* **107,** 16982–16987
22. Komatsu, M., Waguri, S., Chiba, T., Murata, S., Iwata, J., Tanida, I., Ueno, T., Koike, M., Uchiyama, Y., Kominami, E., and Tanaka, K. (2006) Loss of autophagy in the central nervous system causes neurodegeneration in mice. *Nature* **441,** 880–884
23. Hara, T., Nakamura, K., Matsui, M., Yamamoto, A., Nakahara, Y., Suzuki-Migishima, R., Yokoyama, M., Mishima, K., Saito, I., Okano, H., and Mizushima, N. (2006) Suppression of basal autophagy in neural cells causes neurodegenerative disease in mice. *Nature* **441,** 885–889
24. Urushitani, M., Kurisu, J., Tsukita, K., and Takahashi, R. (2002) Proteasomal inhibition by misfolded mutant superoxide dismutase 1 induces selective motor neuron death in familial amyotrophic lateral sclerosis. *J. Neurochem.* **83,** 1030–1042
25. Lee, M., Hyun, D. H., Marshall, K. A., Ellerby, L. M., Bredesen, D. E., Jenner, P., and Halliwell, B. (2001) Effect of overexpression of BCL-2 on cellular oxidative damage, nitric oxide production, antioxidant defenses, and the proteasome. *Free Radic. Biol. Med.* **31,** 1550–1559
26. Casciati, A., Ferri, A., Cozzolino, M., Celsi, F., Nencini, M., Rotilio, G., and Carrì, M. T. (2002) Oxidative modulation of nuclear factor-κB in human cells expressing mutant fALS-typical superoxide dismutases. *J. Neurochem.* **83,** 1019–1029
27. Aquilano, K., Rotilio, G., and Ciriolo, M. R. (2003) Proteasome activation and nNOS down-regulation in neuroblastoma cells expressing a Cu,Zn superoxide dismutase mutant involved in familial ALS. *J. Neurochem.* **85,** 1324–1335
28. Vlug, A. S., and Jaarsma, D. (2004) Long term proteasome inhibition does not preferentially afflict motor neurons in organotypical spinal cord cultures. *Amyotroph. Lateral. Scler Other Motor Neuron. Disord.* **5,** 16–21
29. Kabuta, T., Suzuki, Y., and Wada, K. (2006) Degradation of amyotrophic lateral sclerosis-linked mutant Cu,Zn-superoxide dismutase proteins by macroautophagy and the proteasome. *J. Biol. Chem.* **281,** 30524–30533
30. Urushitani, M., Sato, T., Bamba, H., Hisa, Y., and Tooyama, I. (2010) Synergistic effect between proteasome and autophagosome in the clearance of polyubiquitinated TDP-43. *J. Neurosci. Res.* **88,** 784–797
31. Fornai, F., Longone, P., Cafaro, L., Kastsiuchenka, O., Ferrucci, M., Manca, M. L., Lazzeri, G., Spalloni, A., Bellio, N., Lenzi, P., Modugno, N., Siciliano, G., Isidoro, C., Murri, L., Ruggieri, S., and Paparelli, A. (2008) Lithium delays progression of amyotrophic lateral sclerosis. *Proc. Natl. Acad. Sci. U.S.A.* **105,** 2052–2057
32. Wang, I. F., Guo, B. S., Liu, Y. C., Wu, C. C., Yang, C. H., Tsai, K. J., and Shen, C. K. (2012) Autophagy activators rescue and alleviate pathogenesis of a mouse model with proteinopathies of the TAR DNA-binding protein 43. *Proc. Natl. Acad. Sci. U.S.A.* **109,** 15024–15029
33. Bhattacharya, A., Bokov, A., Muller, F. L., Jernigan, A. L., Maslin, K., Diaz, V., Richardson, A., and Van Remmen, H. (2012) Dietary restriction but not rapamycin extends disease onset and survival of the H46R/H48Q mouse model of ALS. *Neurobiol. Aging* **33,** 1829–1832
34. Wahl, C., Kautzmann, S., Krebiehl, G., Strauss, K., Woitalla, D., Muller, T., Bauer, P., Riess, O., and Krüger, R. (2008) A comprehensive genetic study of the proteasomal subunit S6 ATPase in German Parkinson's disease patients. *J. Neural. Transm.* **115,** 1141–1148
35. Sakao, Y., Kawai, T., Takeuchi, O., Copeland, N. G., Gilbert, D. J., Jenkins, N. A., Takeda, K., and Akira, S. (2000) Mouse proteasomal ATPases Psmc3 and Psmc4: genomic organization and gene targeting. *Genomics* **67,** 1–7
36. Takeuchi, T., Nomura, T., Tsujita, M., Suzuki, M., Fuse, T., Mori, H., and Mishina, M. (2002) Flp recombinase transgenic mice of C57BL/6 strain for conditional gene targeting. *Biochem. Biophys. Res. Commun.* **293,** 953–957
37. Mishina, M., and Sakimura, K. (2007) Conditional gene targeting on the pure C57BL/6 genetic background. *Neurosci. Res.* **58,** 105–112
38. Misawa, H., Nakata, K., Toda, K., Matsuura, J., Oda, Y., Inoue, H., Tateno, M., and Takahashi, R. (2003) VAChT-Cre. Fast and VAChT-Cre.Slow: postnatal expression of Cre recombinase in somatomotor neurons with different onset. *Genesis* **37,** 44–50

39. Sakai, K., and Miyazaki, J. (1997) A transgenic mouse line that retains Cre recombinase activity in mature oocytes irrespective of the cre transgene transmission. *Biochem. Biophys. Res. Commun.* **237,** 318–324
40. Komatsu, M., Wang, Q. J., Holstein, G. R., Friedrich, V. L., Jr., Iwata, J., Kominami, E., Chait, B. T., Tanaka, K., and Yue, Z. (2007) Essential role for autophagy protein Atg7 in the maintenance of axonal homeostasis and the prevention of axonal degeneration. *Proc. Natl. Acad. Sci. U.S.A.* **104,** 14489–14494
41. Koike, M., Shibata, M., Tadakoshi, M., Gotoh, K., Komatsu, M., Waguri, S., Kawahara, N., Kuida, K., Nagata, S., Kominami, E., Tanaka, K., and Uchiyama, Y. (2008) Inhibition of autophagy prevents hippocampal pyramidal neuron death after hypoxic-ischemic injury. *Am. J. Pathol.* **172,** 454–469
42. DeMartino, G. N., Moomaw, C. R., Zagnitko, O. P., Proske, R. J., Chu-Ping, M., Afendis, S. J., Swaffield, J. C., and Slaughter, C. A. (1994) PA700, an ATP-dependent activator of the 20 S proteasome, is an ATPase containing multiple members of a nucleotide-binding protein family. *J. Biol. Chem.* **269,** 20878–20884
43. Kaneko, T., Hamazaki, J., Iemura, S., Sasaki, K., Furuyama, K., Natsume, T., Tanaka, K., and Murata, S. (2009) Assembly pathway of the Mammalian proteasome base subcomplex is mediated by multiple specific chaperones. *Cell* **137,** 914–925
44. Deng, H. X., Chen, W., Hong, S. T., Boycott, K. M., Gorrie, G. H., Siddique, N., Yang, Y., Fecto, F., Shi, Y., Zhai, H., Jiang, H., Hirano, M., Rampersaud, E., Jansen, G. H., Donkervoort, S., Bigio, E. H., Brooks, B. R., Ajroud, K., Sufit, R. L., Haines, J. L., Mugnaini, E., Pericak-Vance, M. A., and Siddique, T. (2011) Mutations in UBQLN2 cause dominant X-linked juvenile and adult-onset ALS and ALS/dementia. *Nature* **477,** 211–215
45. Yamanaka, K., Chun, S. J., Boillee, S., Fujimori-Tonou, N., Yamashita, H., Gutmann, D. H., Takahashi, R., Misawa, H., and Cleveland, D. W. (2008) Astrocytes as determinants of disease progression in inherited amyotrophic lateral sclerosis. *Nat. Neurosci.* **11,** 251–253
46. Papadeas, S. T., Kraig, S. E., O'Banion, C., Lepore, A. C., and Maragakis, N. J. (2011) Astrocytes carrying the superoxide dismutase 1 (SOD1G93A) mutation induce wild-type motor neuron degeneration in vivo. *Proc. Natl. Acad. Sci. U.S.A.* **108,** 17803–17808
47. Urushitani, M., Ezzi, S. A., and Julien, J. P. (2007) Therapeutic effects of immunization with mutant superoxide dismutase in mice models of amyotrophic lateral sclerosis. *Proc. Natl. Acad. Sci. U.S.A.* **104,** 2495–2500
48. Bjørkøy, G., Lamark, T., Brech, A., Outzen, H., Perander, M., Overvatn, A., Stenmark, H., and Johansen, T. (2005) p62/SQSTM1 forms protein aggregates degraded by autophagy and has a protective effect on huntingtin-induced cell death. *J. Cell Biol.* **171,** 603–614
49. Kirkin, V., Lamark, T., Sou, Y. S., Bjørkøy, G., Nunn, J. L., Bruun, J. A., Shvets, E., McEwan, D. G., Clausen, T. H., Wild, P., Bilusic, I., Theurillat, J. P., Øvervatn, A., Ishii, T., Elazar, Z., Komatsu, M., Dikic, I., and Johansen, T. (2009) A role for NBR1 in autophagosomal degradation of ubiquitinated substrates. *Mol. Cell* **33,** 505–516
50. Wang, X., Fan, H., Ying, Z., Li, B., Wang, H., and Wang, G. (2010) Degradation of TDP-43 and its pathogenic form by autophagy and the ubiquitin-proteasome system. *Neurosci. Lett.* **469,** 112–116
51. Ciechanover, A., and Brundin, P. (2003) The ubiquitin proteasome system in neurodegenerative diseases: sometimes the chicken, sometimes the egg. *Neuron* **40,** 427–446
52. Lee, J. A. (2012) Neuronal autophagy: a housekeeper or a fighter in neuronal cell survival? *Exp. Neurobiol.* **21,** 1–8
53. Zhang, X., Li, L., Chen, S., Yang, D., Wang, Y., Zhang, X., Wang, Z., and Le, W. (2011) Rapamycin treatment augments motor neuron degeneration in SOD1(G93A) mouse model of amyotrophic lateral sclerosis. *Autophagy* **7,** 412–425
54. Droggiti, A., Ho, C. C., Stefanis, L., Dauer, W. T., and Rideout, H. J. (2011) Targeted disruption of neuronal 19S proteasome subunits induces the formation of ubiquitinated inclusions in the absence of cell death. *J. Neurochem.* **119,** 630–643
55. McNaught, K. S., Belizaire, R., Jenner, P., Olanow, C. W., and Isacson, O. (2002) Selective loss of 20S proteasome α-subunits in the substantia nigra pars compacta in Parkinson's disease. *Neurosci. Lett.* **326,** 155–158
56. Lang-Rollin, I., Vekrellis, K., Wang, Q., Rideout, H. J., and Stefanis, L. (2004) Application of proteasomal inhibitors to mouse sympathetic neurons activates the intrinsic apoptotic pathway. *J. Neurochem.* **90,** 1511–1520
57. Lang-Rollin, I., Maniati, M., Jabado, O., Vekrellis, K., Papantonis, S., Rideout, H. J., and Stefanis, L. (2005) Apoptosis and the conformational change of Bax induced by proteasomal inhibition of PC12 cells are inhibited by bcl-xL and bcl-2. *Apoptosis* **10,** 809–820
58. Rideout, H. J., Lang-Rollin, I. C., Savalle, M., and Stefanis, L. (2005) Dopaminergic neurons in rat ventral midbrain cultures undergo selective apoptosis and form inclusions, but do not up-regulate iHSP70, following proteasomal inhibition. *J. Neurochem.* **93,** 1304–1313
59. Kim, S. H., Shanware, N. P., Bowler, M. J., and Tibbetts, R. S. (2010) Amyotrophic lateral sclerosis-associated proteins TDP-43 and FUS/TLS function in a common biochemical complex to co-regulate HDAC6 mRNA. *J. Biol. Chem.* **285,** 34097–34105
60. Bentmann, E., Neumann, M., Tahirovic, S., Rodde, R., Dormann, D., and Haass, C. (2012) Requirements for Stress Granule Recruitment of Fused in Sarcoma (FUS) and TAR DNA-binding Protein of 43 kDa (TDP-43). *J. Biol. Chem.* **287,** 23079–23094
61. Maragakis, N. J., and Rothstein, J. D. (2006) Mechanisms of Disease: astrocytes in neurodegenerative disease. *Nat. Clin. Pract. Neurol.* **2,** 679–689